Journal of the European Ceramic Society xxx (2016) xxx–xxx

Contents lists available at www.sciencedirect.com

Journal of the European Ceramic Society

journal homepage: www.elsevier.com/locate/jeurceramsoc

Crystal structure and microwave dielectric characteristics of Zr-substituted $CoTiNb_2O_8$ ceramics

Yun Zhang, Yingchun Zhang*, Maoqiao Xiang

School of Materials Science and Engineering, University of Science and Technology Beijing, 100083 Beijing, PR China

ARTICLE INFO

Article history:
Received 30 November 2015
Received in revised form 11 February 2016
Accepted 12 February 2016
Available online xxx

Keywords:
$Co(Ti_{1-x}Zr_x)Nb_2O_8$ ceramic
Sintering
Crystal structure
Microwave dielectric property

ABSTRACT

$Co(Ti_{1-x}Zr_x)Nb_2O_8$ microwave dielectric ceramics were synthesized via the conventional solid-state reaction route. The dependence of microwave dielectric properties on the crystal structure was discussed. The phase transitions were analyzed using X-ray powder diffraction, Raman spectroscopy, and transmission electron microscopy. A series of composition-induced phase transitions were confirmed via the sequence: tetragonal rutile structure → coexistence of rutile and wolframite phase → monoclinic wolframite structure. For the $Co(Ti_{1-x}Zr_x)Nb_2O_8$ compounds, Zr substitutions from 0 to 1 led to a decrease in the ε_r from 62.4 to 23.8. In contrast to ε_r, $Q \times f$ increased considerably, which was explained in terms of packing fraction. The τ_f was correlated with oxygen octahedral distortion and B-site bond valence. A near zero τ_f of 4.4 ppm/°C was obtained in the $CoTi_{0.4}Zr_{0.6}Nb_2O_8$ ceramics with an ε_r of 29.9 and a high $Q \times f$ of 72,833 GHz.

1. Introduction

The rapid progress in mobile and satellite communication system in the last decades has stimulated the development of microwave dielectric ceramics, which are widely used as microwave components such as filters, resonators, wave guides, etc. [1,2] With respect to specific microwave applications, such materials are basically required to possess a range of dielectric properties, including appropriate dielectric constant (ε_r), high quality factor ($Q \times f$), and near-zero temperature coefficient of resonant frequency (τ_f) [3]. Achieving all the above-mentioned characteristics in one material is a formidable task. The search for new materials with desired properties has been ongoing.

Recently, $M^{2+}M^{4+}Nb_2O_8$ (M^{2+} = Mg, Ca, Mn, Co, Ni, Zn and M^{4+} = Ti, Zr) ceramics are very attractive subjects for materials research and engineering applications. They were first investigated by Baumgarte and Blachnik [4]. Depending on the differences between the radii of M^{2+} and M^{4+} cations, three structure types, i.e. rutile, wolframite and ixiolite were described. Later on, numerous studies were conducted on $M^{2+}M^{4+}Nb_2O_8$ compositions because of their flexibility for the substitution of different cations to obtain favorable dielectric properties. The ε_r values were found in the range of 9.6–71.2, accompanied by relatively low dielectric loss [5–8]. The microwave dielectric properties of rutile structure $NiTiNb_2O_8$, for instance, were accomplished by Liao et al. and reported to have an ε_r of 56.8, a $Q \times f$ of 21,100 GHz, and a τ_f of 79.1 ppm/°C [6].

$CoTiNb_2O_8$ ceramic was also rutile type in the $M^{2+}M^{4+}Nb_2O_8$ family and belonged to the tetragonal crystal system with space group *P*42/*mnm*. Tseng [7] demonstrated this material exhibited a medium ε_r of 64 and a high $Q \times f$ of 65,300 GHz after sintering at 1120 °C. However, the τ_f (~223.2 ppm/°C) was poor for practical applications. It was possible to prepare temperature-stable ceramics by combining two compatible compounds with opposite τ_f or forming solid solution. For example, tunability of τ_f had been done in the $Sr(Ga_{0.5}Nb_{0.5})_{1-x}Ti_xO_3$ perovskite solid solution [9]. Nevertheless, few studies about the performance improvement of $CoTiNb_2O_8$ ceramic were reported until 2013. Huan et al. [10] outlined zero τ_f was achieved by partial replacement of cobalt with equivalent-charge zinc, but unfortunately the $Q \times f$ was deteriorated by one half. The radius of Zr^{4+} (0.72 Å, CN = 6) was similar to Ti^{4+} (0.605 Å, CN = 6) [11], Zr substitution for Ti could effectively adjust the τ_f without detrimental effect on $Q \times f$ values, such as in the $Zn_{0.5}Ti_{1-x}Zr_xNbO_4$ and $CaLa_4(Zr_xTi_{1-x})_4O_{15}$ systems [12,13]. Thus, the microwave dielectric properties of $CoTiNb_2O_8$ system were likely to be enhanced by introducing Zr since most of the zirconia-based materials had negative τ_f values [5].

In this work, $Co(Ti_{1-x}Zr_x)Nb_2O_8$ (x = 0–1) ceramics were synthesized by high-temperature solid state reaction technique. And

* Corresponding author. Fax: +86 1062334951.
E-mail addresses: zycustb@163.com, zhang@ustb.edu.cn (Y. Zhang).

http://dx.doi.org/10.1016/j.jeurceramsoc.2016.02.026
0955-2219/

the correlation between crystal structure and microwave dielectric properties was also investigated.

2. Experimental procedures

$Co(Ti_{1-x}Zr_x)Nb_2O_8$ ($x = 0, 0.2, 0.4, 0.6, 0.8, 1$) ceramics were synthesized by conventional solid state reaction route. High-purity oxide powders (>99.9%) of CoO, TiO_2, ZrO_2 and Nb_2O_5 were adopted as raw chemicals. Stoichiometric amounts of the oxides were weighed and mixed with ethanol in polyethylene bottles. Subsequently, the slurries were rapidly dried and calcined at 1100 °C for 4 h in air with a heating rate of 5 °C/min. After remilling and sieving through 100 mesh, the powders together with the organic binder (5 wt% polyvinyl alcohol) were uniaxially compacted into cylinders of 10 mm in diameter and 6 mm in thickness at a pressure of 150 MPa. The green bodies were heated at 500 °C for 2 h to remove the organic binder and then sintered in the temperature range of 1200–1450 °C for 4 h in air. The heating rate and the cooling rate were both maintained at 2 °C/min.

The relative densities of the sintered samples were identified by Archimedes method. Crystal structure was undertaken by X-ray diffraction (XRD, Rigaku, DMAX-RB, Japan) with Cu$K\alpha$ radiation. The structural parameters were obtained from Rietveld refinement of the XRD data using GSAS-EXPGUI program [14]. Raman spectroscopy was performed using a LabRam HR (Jobin-Yvon, France). The 514.5 nm line of an Ar-ion laser was used as the excitation source. Selected area electron diffraction (SAED) patterns were recorded in a transmission electron microscopy (TEM-2100, JEOL, Tokyo, Japan), operating at 200 kV. Microstructure of the sintered compacts was observed with scanning electron microscope (SEM, JSM-6480LV). For microstructure observation, these samples were polished with 1 μm diamond paste, and then thermally etched at 100 °C below the optimal sintering temperature for 30 min. The microwave dielectric properties of the samples were evaluated by a network analyzer (HP8720ES, Hewlett-Packard, Santa, Rosa, CA). The dielectric constant was measured using the Hakki–Coleman post-resonator method [15] by exciting the TE_{011} resonant mode of the DR using the electric probe of an antenna as suggested by Courtney [16]. The unloaded quality factors were measured using the $TE_{01\delta}$ mode in the cavity method [17]. All measurements were made in the frequency range of 4–9 GHz at room temperature. Temperature coefficients of the resonant frequencies of the TE_{011} mode were obtained in the temperature range from 25 °C to 80 °C. The τ_f values were defined by the following relationship:

$$\tau_f = \frac{f_2 - f_1}{f_1(T_2 - T_1)} \quad (1)$$

where f_1 and f_2 were the resonant frequency at T_1 and T_2, respectively.

3. Results and discussions

3.1. Relative density

The relative densities of $Co(Ti_{1-x}Zr_x)Nb_2O_8$ ceramics are offered in Fig. 1. For each composition, the relative densities initially increased with increasing temperature and then decreased after reaching a maximum value. With a small amount of Zr-substitution, the maximum relative densities dramatically reduced down to 94.17% at $x = 0.4$. This indicated that partial Zr-substitution decreased the sinterability of samples. Further, the optimal sintering temperatures of samples at which the maximum densities were obtained, increased from 1250 to 1400 °C with the increase of x from 0 to 1. Previous literature revealed that replacement of Ti^{4+} by Zr^{4+} in $SrLa_4Ti_5O_{17}$ ceramics increased the sintering temperature also [18].

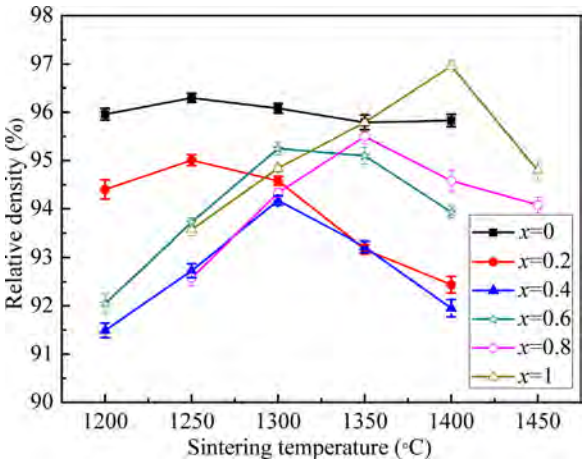

Fig. 1. Relative densities of $Co(Ti_{1-x}Zr_x)Nb_2O_8$ ceramics as a function of sintering temperature.

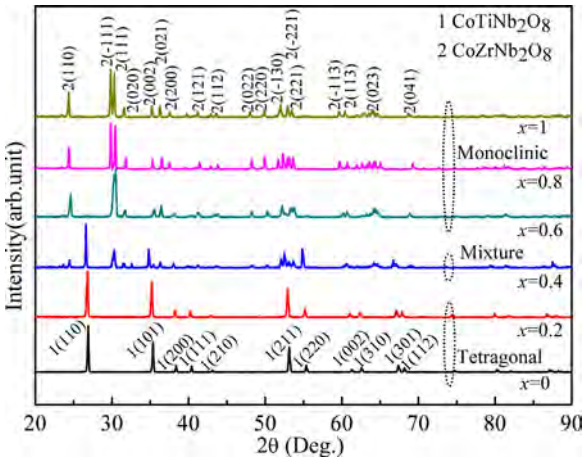

Fig. 2. XRD patterns of $Co(Ti_{1-x}Zr_x)Nb_2O_8$ ceramics sintered at 1300 °C.

3.2. Multiphase refinement and quantitative determination

Fig. 2 shows the XRD patterns of $Co(Ti_{1-x}Zr_x)Nb_2O_8$ ceramics sintered at 1300 °C. The ceramics were crystallized in tetragonal rutile structure (JCPDS NO. 52-1875) when $x \leq 0.2$. However, in the compositions of $x = 0.6$–1, all patterns could be indexed as the monoclinic wolframite-structure with space group $P2/c$. For $x = 0.4$, the nominal composition was $CoTi_{0.6}Zr_{0.4}Nb_2O_8$. It did not form a single phase, but rather a mixture of rutile and wolframite phase. Rietveld refinement was used to analyze the structure evolution in the $Co(Ti_{1-x}Zr_x)Nb_2O_8$ system (Table 1).The refinement involved lattice parameters, background, atomic coordinates, site occupancies and isotropic thermal parameters as well as profile parameters (peak height and peak shape). The $Zn_{0.15}Nb_{0.30}Ti_{0.55}O_2$ reported by Abrahams [19] and $CdWO_4$ reported by Daturi [20] were adopted as the starting models. A part of the refinement results for $Co(Ti_{1-x}Zr_x)Nb_2O_8$ such as lattice parameters and bond length are listed in Tables 1 and 2. From the refinement results, it was found that there was an expansion in the unit cell volume with Zr-substitution.

3.3. Structure analysis

$CoTiNb_2O_8$ performed tetragonal rutile structure which belonged to space group $P42/mnm$. Like α-PbO_2-type structure, rutile-type structure also consisted of close-packed oxygen layers,

Please cite this article in press as: Y. Zhang, et al., Crystal structure and microwave dielectric characteristics of Zr-substituted $CoTiNb_2O_8$ ceramics, *J Eur Ceram Soc* (2016), http://dx.doi.org/10.1016/j.jeurceramsoc.2016.02.026

Table 1
Crystallograghic data obtained from Rietveld refinement for $Co(Ti_{1-x}Zr_x)Nb_2O_8$ ceramics.

x (mol)	Lattice parameters					V_{unit} (Å^3)	Reliability factors
	a(Å)	b(Å)	c(Å)	$\alpha=\gamma$	β		R_{wp}(%), R_p(%), X^2
(a) $CoTiNb_2O_8$							
0	4.7122(1)	4.7122(1)	3.1282(7)	90	90	69.4629(9)	9.1, 8.2, 1.11
0.2	4.7120(3)	4.7120(3)	3.1302(1)	90	90	69.5007(6)	8.9, 7.6, 1.17
0.4	4.7139(2)	4.7139(2)	3.1322(6)	90	90	69.6020(8)	10.1, 8.7, 1.16
(b) $CoZrNb_2O_8$							
0.4	4.7852(2)	5.6602(5)	5.0925(4)	90	91.0422(7)	137.9113(1)	9.3, 8.1, 1.15
0.6	4.7861(3)	5.6617(4)	5.0922(2)	90	91.0520(1)	137.9647(6)	9.6, 8.4, 1.14
0.8	4.7858(6)	5.6649(8)	5.0921(1)	90	91.0445(2)	138.0333(6)	9.0, 8.2, 1.10
1	4.7859(1)	5.6653(4)	5.0935(2)	90	91.0477(2)	138.0816(6)	9.4, 8.3, 1.13

R_{wp}-reliability factor of weighted pattern; R_p-reliability factor of patterns; χ^2-goodness of fit indicator.

in which the cations occupied half of the octahedral sites and the occupied octahedra shared edges, thus forming infinite linear chains in the c-direction. However, in the rutile-type structure, the edge-sharing octahedra chains were straight instead of zigzagged [4].

With substitution of Zr, the atomic interactions in $Co(Ti_{1-x}Zr_x)Nb_2O_8$ ceramics were elongated or compressed inevitably, which finally gave rise to structural changes. The distortion of oxygen octahedral and bond valence of Nb-site calculated from Rietveld Refinement are summarized in Table 2. From the individual bond length of oxygen octahedral, the octahedral distortion of tetragonal rutile structure was calculated from Eq. (2) [11]:

$$\text{Octahedral distortion}(\Delta) = \frac{1}{6}\Sigma\left\{\frac{R_i - \bar{R}}{\bar{R}}\right\}^2 \quad (2)$$

where R_i was an individual bond length, and $\bar{R}$ was the average bond length of oxygen octahedron.

The bond valence of atom i, V_{ij} was defined as the sum of all of the valences from a given atom i, as calculated from Eqs. (3) and (4) [21]:

$$V_{ij} = \Sigma v_{ij} \quad (3)$$

$$v_{ij} = \exp\left(\frac{R_{ij-d_{ij}}}{b\prime}\right) \quad (4)$$

where R_{ij} was the bond valence parameter, d_{ij} was the length of a bond between atoms i and j, and b' was commonly taken to be a universal constant equal to 0.37 Å. The bond valence parameters followed the values in the previous report [22].

In the structure of $CoZrNb_2O_8$, all the A-site (Co^{2+}, Zr^{4+}) and B-site (Nb^{5+}) cations were octahedrally coordinated with oxygen anions and occupied the 2f and 2e Wyckoff positions, respectively. Two different oxygen anions (O1 and O2) occupied the 4 g Wyckoff positions. O1 was connected to one B-site (Nb^{5+}) cation and two A-site (Co^{2+}/Zr^{4+}) cations, with short (1.78 Å) and relatively longer (2.25 Å) bonds respectively, whereas another oxygen O2 was bonded with one A-site and two B-site cations. [4,5]

In this case, the distortion of an octahedron was defined as [23]:

$$\text{Octahedral distortion}(\Delta) = \frac{\text{B}-\text{O distance}_{\text{largest}} - \text{B}-\text{O distance}_{\text{smallest}}}{\text{B}-\text{O distance}_{\text{average}}} \quad (5)$$

3.4. Raman analysis

Raman spectroscopy was very sensitive to the variation of crystal structure induced by cation substitution or processing condition.

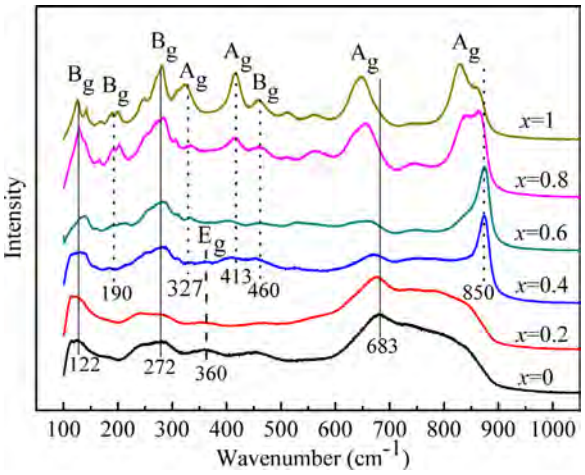

Fig. 3. Raman spectra of $Co(Ti_{1-x}Zr_x)Nb_2O_8$ ceramics sintered at 1300 °C.

Herein, Raman spectroscopy was also employed to characterize the phase composition of $Co(Ti_{1-x}Zr_x)Nb_2O_8$ samples. According to the group theoretical calculations, the Raman-active phonon modes of rutile structure were $A_g + 2B_g + E_g$, while those of the monoclinic structure were given by $9A_g + 12B_g$ [24]. Actually, only few bands are detected in Fig. 3 since some weak vibration modes were broadened and overlapped. For $x = 0$, three basic modes were attributed as follows: 122 cm^{-1} to lattice vibration; 272 cm^{-1} to CoO_6 octahedra stretching deformation and 683 cm^{-1} to Nb—O symmetric vibration [25,26]. These modes were observed clearly up to $x = 1$. When transition took place from rutile to monoclinic, the E_g mode caused by Ti—O stretching vibration disappeared at 360 cm^{-1} [27]. Meanwhile, the Zr—O symmetric vibration mode at 850 cm^{-1} was the most prominent peak [24]. Beyond that, four extra Raman modes started to appear, of which two modes at 190 and 413 cm^{-1} were assigned to Zr—O stretching vibration [28], whereas the two remaining Raman modes stemmed probably from O—Zr—O bending [29]. Along with these changes, two more features were explicitly noticed in the Raman spectra. One was the shifting of A_g mode around 683 cm^{-1} and the other was the splitting of the Zr—O symmetric stretching mode. With the addition of Zr, the unit cell volume increased which in turn affected the interatomic distances in the NbO_6 octahedron and caused the decrease in the covalence of bond between cation and NbO_6 [30]. Out of these effects, the A_g mode shifted to lower wave number side. On the other hand, the splitting observed in Raman spectroscopies was likely ascribed to the electronegativity difference between Zr(1.33) and Ti(1.54) atoms present at the same site [31,32]. The lower electronegativity of Zr resulted in the formation of highly covalent bond with oxygen in comparison with Ti—O bond.

Please cite this article in press as: Y. Zhang, et al., Crystal structure and microwave dielectric characteristics of Zr-substituted $CoTiNb_2O_8$ ceramics, J Eur Ceram Soc (2016), http://dx.doi.org/10.1016/j.jeurceramsoc.2016.02.026

Table 2
Nb-site bond valence and oxygen octahedral distortion in $Co(Ti_{1-x}Zr_x)Nb_2O_8$ ceramics.

x (mol)	d_{NbO} (Å)	R_{NbO}	v_{NbO}	V_{NbO}	$\Delta_{octahedral}$	τ_f (ppm/°C)
(a)$CoTiNb_2O_8$						
0	2.2187(8) × 2	1.911	0.4352 × 2	2.5183	0.73×10^{-4}	76.6
	2.2597(5) × 2		0.3896 × 2			
	2.2196(2) × 2		0.4343 × 2			
0.2	2.2145(8) × 2	1.911	0.4402 × 2	2.5304	0.86×10^{-4}	59.8
	2.2602(2) × 2		0.3891 × 2			
	2.2182(6) × 2		0.4359 × 2			
0.4	2.2147(4) × 2	1.911	0.4400 × 2	2.5320	0.98×10^{-4}	30.4
	2.2621(7) × 2		0.3871 × 2			
	2.2157(1) × 2		0.4389 × 2			
(b)$CoZrNb_2O_8$						
0.4	1.9067(3) × 2	1.911	1.0116 × 2	4.4896	11.27%	30.4
	2.0492(6) × 2		0.6882 × 2			
	2.1355(7) × 2		0.5450 × 2			
0.6	1.9062(2) × 2	1.911	1.0130 × 2	4.4993	11.30%	4.4
	2.0473(8) × 2		0.6917 × 2			
	2.1356(1) × 2		0.5450 × 2			
0.8	1.9047(2) × 2	1.911	1.0171 × 2	4.5069	11.51%	−15.7
	2.0454(9) × 2		0.6952 × 2			
	2.1382(4) × 2		0.5411 × 2			
1	1.9033(7) × 2	1.911	1.0208 × 2	4.5145	11.62%	−29.4
	2.0448(2) × 2		0.6965 × 2			
	2.1390(5) × 2		0.5399 × 2			

3.5. TEM analysis

In order to confirm the coexistence of the wolframite and rutile phases at $x = 0.4$, $CoTi_{0.6}Zr_{0.4}Nb_2O_8$ ceramic was thinned by ion milling and analyzed by TEM. A typical TEM bright field image is shown in Fig. 4(a). The selected area electron diffraction (SAED) patterns obtained for the two positions of A and B in the bright field image are given in Fig. 4 (b) and (c), respectively. By indexing the SAED patterns, the structures were found to be tetragonal and monoclinic for the position A and B, respectively. We could not observe any other phases at all. Thus, the XRD analysis and Raman spectra were further substantiated by the TEM results.

3.6. Morphological analysis

Fig. 5 illustrates the SEM images of the thermally etched surfaces of $Co(Ti_{1-x}Zr_x)Nb_2O_8$ ($0 \le x \le 1$) ceramics sintered at respective optimum temperatures. The grain size and the amount of pores were greatly affected by sintering temperature and composition. For $0 \le x \le 0.2$, the $Co(Ti_{1-x}Zr_x)Nb_2O_8$ samples sintered at 1250 °C depicted a distribution of 2–11 μm grain size and an appreciable amount of intergranular porosity. Whereas for $x = 0.4$ in Fig. 5(c), the specimen exhibited a porous microstructure even though at its optimum sintering temperature, probably because of the specific composition. At $x = 0.4$, the generated $CoZrNb_2O_8$ existed as a second phase, which pinned the grain boundaries and eventually inhibited the grain growth. From $x = 0.6$ onwards, the grain size increased observably, attributing to the increased optimum sintering temperature. As x increased to 1, a uniform microstructure with closely packed polygonal grains having 10–15 μm size was developed [Fig. 5(f)].

3.7. Microwave dielectric properties

The dielectric constants of the $Co(Ti_{1-x}Zr_x)Nb_2O_8$ ceramics sintered at different temperatures are depicted in Fig. 6. By increasing the sintering temperature, the dielectric constants of all compositions increased to maximum values, corresponding to the optimum densification temperature, and declined thereafter. With a minor Zr addition ($0 \le x \le 0.4$), the dielectric constants fell rapidly to 46.3, following somewhat similar trend as that of relative density in Fig. 1. This was not difficult to accept because some of early researches had proved the influence of relative density on the dielectric properties [7,8]. Upon further increasing Zr content, the ε_r values continued to decrease, independent of the observed relative densities. To clarify the effects of Zr substitution on the dielectric constant, theoretical dielectric polarizability ($\alpha_{theo.}$) was obtained from the additive rule [33] as formulated in Eq. (6). Additionally, the observed dielectric polarizability ($\alpha_{obs.}$) was determined using the Clausiuse–Mossotti Eq. (7) [33].

$$\alpha_{theo.} = \alpha(CoTi_{1-x}Zr_xNb_2O_8)$$

$$= \alpha(Co) + (1-x)\alpha(Ti) + x\alpha(Zr) + 2\alpha(Nb) + 8\alpha(O) \quad (6)$$

$$\alpha_{obs.} = \frac{V_m(\varepsilon_r - 1)}{b(\varepsilon_r + 2)} \quad (7)$$

where α(Co), α(Ti), α(Zr), α(Nb) and α(O) represented ions polarizabilities reported by Shannon; V_m, ε_r and b indicated the molar volume of samples, dielectric constant and constant value ($4\pi/3$),

Table 3
Comparison of observed and theoretical polarizabilities of $Co(Ti_{1-x}Zr_x)Nb_2O_8$ specimens sintered at 1300 °C.

x (mol)	Weight fraction of $CoTiNb_2O_8$ (%)	Volume fraction of $CoTiNb_2O_8$ (%)	Theoretical $\alpha_{theo.}$	Observed	
				ε_r	$\alpha_{obs.}$
0	100	100	28.63	58.8	31.53
0.2	100	100	28.69	54.1	31.41
0.4	51.54	52.96	28.75	46.3	31.03
0.6	–	–	28.83	29.9	29.84
0.8	–	–	28.88	25.2	29.32
1	–	–	28.92	22.1	28.86

Please cite this article in press as: Y. Zhang, et al., Crystal structure and microwave dielectric characteristics of Zr-substituted $CoTiNb_2O_8$ ceramics, *J Eur Ceram Soc* (2016), http://dx.doi.org/10.1016/j.jeurceramsoc.2016.02.026

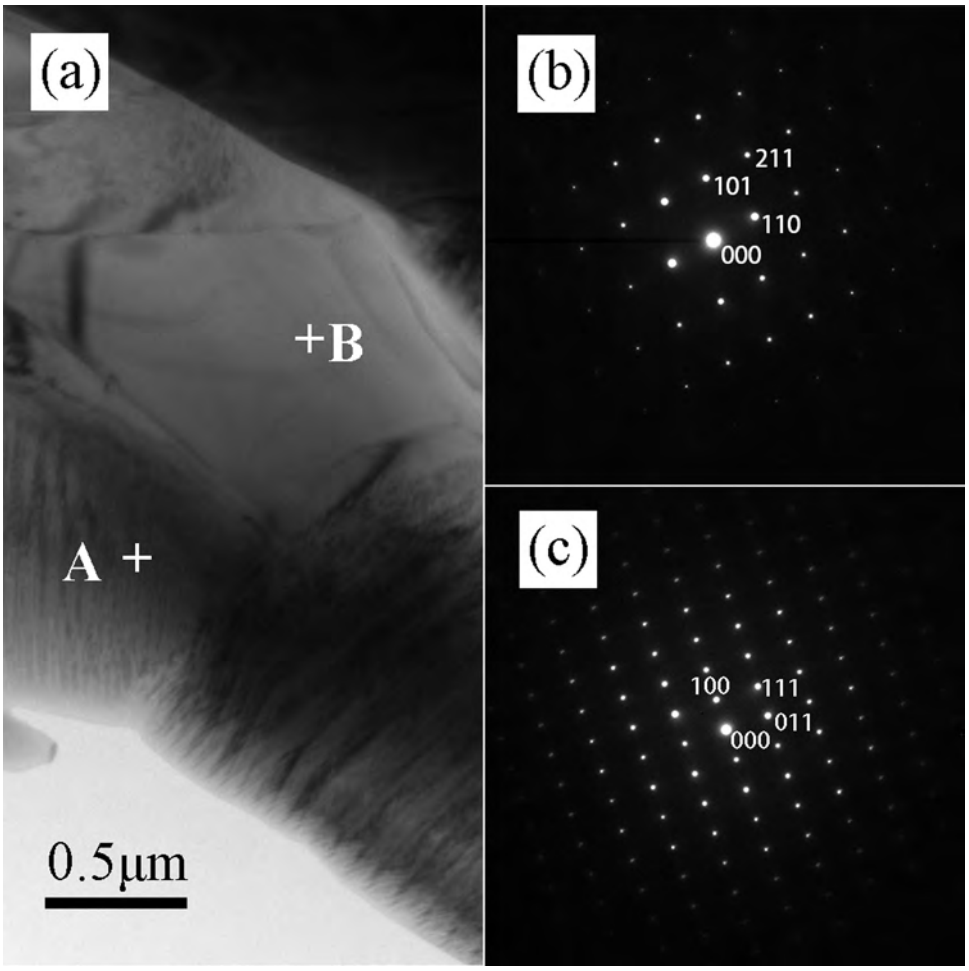

Fig. 4. (a) TEM bright field image of $CoTi_{0.6}Zr_{0.4}Nb_2O_8$ ceramics sintered at 1300 °C; (b) and (c) are SAED patterns of position A and B in (a), respectively.

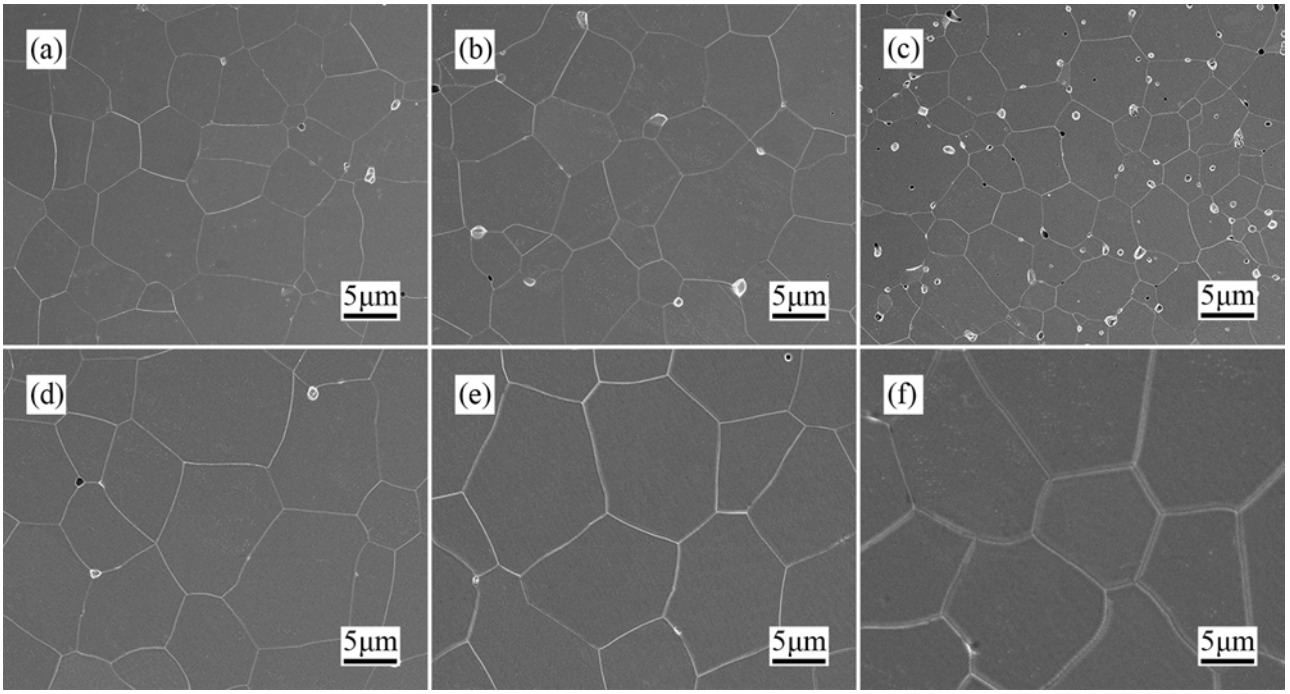

Fig. 5. SEM images of polished and thermally etched $Co(Ti_{1-x}Zr_x)Nb_2O_8$ ceramics sintered at different temperatures for 4 h: (a) $x = 0$, at 1250 °C; (b) $x = 0.2$, at 1250 °C; (c) $x = 0.4$, at 1300 °C; (d) $x = 0.6$, at 1300 °C; (e) $x = 0.8$, 1350 °C; and (f) $x = 1$, at 1400 °C.

Please cite this article in press as: Y. Zhang, et al., Crystal structure and microwave dielectric characteristics of Zr-substituted $CoTiNb_2O_8$ ceramics, *J Eur Ceram Soc* (2016), http://dx.doi.org/10.1016/j.jeurceramsoc.2016.02.026

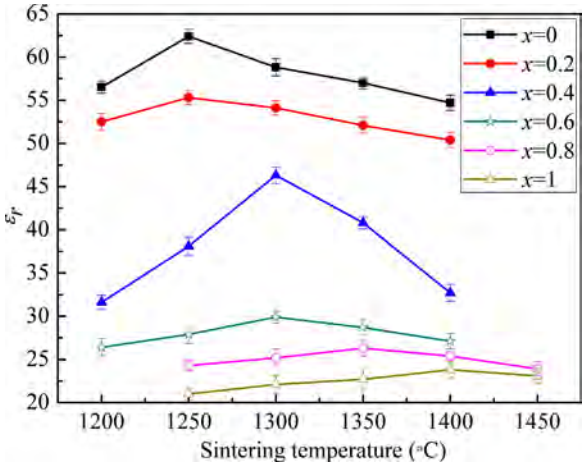

Fig. 6. Dielectric constants of $Co(Ti_{1-x}Zr_x)Nb_2O_8$ ceramics as a function of sintering temperature.

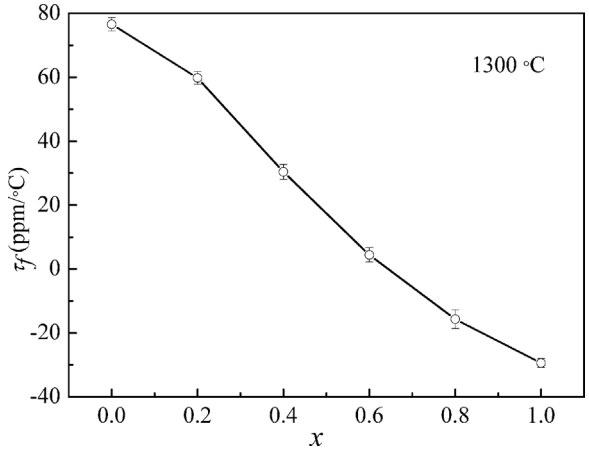

Fig. 8. Temperature coefficients of resonant frequency of $Co(Ti_{1-x}Zr_x)Nb_2O_8$ ceramics sintered at 1300 °C for 4 h.

respectively. Keeping in view the larger ionic dielectric polarizability of Zr (3.25 Å) than Ti(2.93 Å), ε_r should increase with increase in Zr content, but in the present study ε_r decreased, as shown in Table 3. The deviation of $\alpha_{obs.}$ from $\alpha_{theo.}$ might lie in the fact that the ionic polarizabilities used here were all empirically calculated from many series of oxides, the oxide additivity rule could only give some approximate results. The decrease in ε_r mainly resulted from the increase of Nb-site bond valence (see Table 2). The strengthening of V_{Nb-O} decreased the contribution of rattling effect of B-site ion to the polarizabilities of the specimens [34]. Accordingly, the ε_r values decreased steadily. Kato et al. [35] reported that in complex perovskites, the dielectric constant decreased with the increase of effective ionic radius. Thus, the decreased ε_r values were also explained on the basis of the smaller ionic radius of Ti^{4+} compared with Zr^{4+}.

Fig. 7 illustrates the $Q \times f$ values of $Co(Ti_{1-x}Zr_x)Nb_2O_8$ ceramics. The microwave dielectric loss was mainly caused not only by the intrinsic loss such as lattice vibration modes, but also by the extrinsic losses such as density, secondary phases, grains sizes, and lattice defect [36]. Here, the $Q \times f$ values increased gradually with increasing Zr content except for $x = 0.4$, which exhibited lower $Q \times f$ value than its neighboring compositions. The sudden drop in $Q \times f$ at $x = 0.4$ was interpreted as a result of porous structure [Fig. 5(c)]. With the decrease of porosity, the $Q \times f$ value would certainly increase. Once the as-prepared samples were of nearly full density, $Q \times f$ values were markedly affected by intrinsic factors.

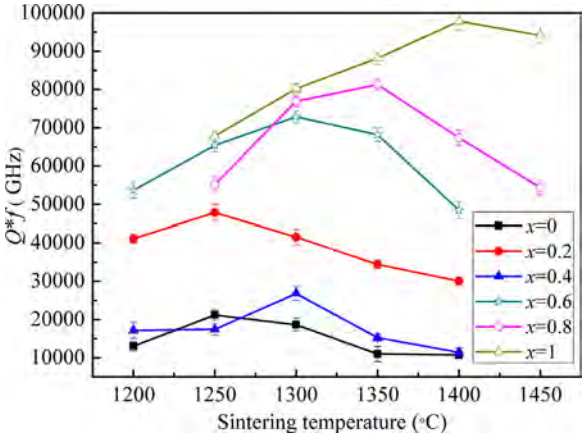

Fig. 7. Quality factors of $Co(Ti_{1-x}Zr_x)Nb_2O_8$ ceramics as a function of sintering temperature.

It was well recognized that the dielectric loss at microwave frequency was directly linked to the packing fraction of the structure [37]. As the packing fraction increased, there would be a reduction in the lattice vibrations, and this tended to increase the $Q \times f$. Based on the crystal structural considerations, the packing fraction of $Co(Ti_{1-x}Zr_x)Nb_2O_8$ ceramics was obtained from Eq. (8):

$$\text{Packing fraction}(\%) = \frac{\text{Volume of the atoms in the cell}}{\text{Volume of primitive unit cell}} \quad (8)$$

As confirmed in Table 4, the variation of $Q \times f$ was consistent with that of packing fraction except for $x = 0.4$ composition. Therefore, the increment in $Q \times f$ was associated mostly with the packing fraction. Obviously, the sintering temperature and loss factor of pure $CoTiNb_2O_8$ ceramics in our study exhibited some differences from the measurements in Ref. [7]. It was inferred that the differences had been made were from the starting raw chemicals.

As for the temperature coefficient of the resonant frequency (τ_f), it was usually related to the structural characteristics. It had been reported earlier that B-site bond valence was a function of bond strength and distance between B-site cation and oxygen [22]. With the increase of B-site bond valence, the bond strength between B-site cation and oxygen and/or the degree of tilting on oxygen octahedral increased. Eventually, the restoring force to the tilting recovers increased, thereby resulting in decreased τ_f. As presented in Table 2 and Fig. 8, the τ_f moved to the negative direction, primarily depending on the increase of Nb-site bond valence and oxygen octahedral distortion. In particular, a near-zero τ_f value of 4.4 ppm/°C was obtained at $x = 0.6$.

4. Conclusions

Crystal structure and microwave dielectric properties of $Co(Ti_{1-x}Zr_x)Nb_2O_8$ ($x = 0$-1) ceramics were studied in this article. Compositionally induced phase transition was analyzed using a combination of X-ray diffraction, FT-Raman and TEM. The system

Table 4
Relationship between structures and $Q \times f$ of $Co(Ti_{1-x}Zr_x)Nb_2O_8$ specimens sintered at 1300 °C.

x (mol)	Packing fraction (%)	$Q \times f$ (GHz)
0	64.00	18,653
0.2	64.06	41,541
0.4	64.34	26,811
0.6	64.82	72,833
0.8	64.88	76,921
1	64.95	80,233

Please cite this article in press as: Y. Zhang, et al., Crystal structure and microwave dielectric characteristics of Zr-substituted $CoTiNb_2O_8$ ceramics, *J Eur Ceram Soc* (2016), http://dx.doi.org/10.1016/j.jeurceramsoc.2016.02.026

remained tetragonal rutile phase when $x \leq 0.2$, and for $x \geq 0.6$, a monoclinic wolframite-type structure was observed, whereas for $x = 0.4$, $CoZrNb_2O_8$ phase coexisted with rutile phase. With the substitution of Zr at Ti-site, the ε_r decreased owing to the decrease of rattling effect of B-site ions. The variation of $Q \times f$ was largely dependent on the packing fraction as well as relative density. Due to the increase of B-site bond valence and oxygen octahedron distortion, the τ_f moved to the negative direction. Typically, $CoTi_{0.4}Zr_{0.6}Nb_2O_8$ ceramics exhibited a well-sintered microstructure with $\varepsilon_r = 29.9$, $Q \times f = 72{,}833$ GHz, and $\tau_f = 4.4$ ppm/°C at $T_s = 1300$ °C.

Acknowledgment

This work has been sponsored by the National Natural Science Foundation of China (Nos. 51372017 and 51172019).

References

[1] C.L. Huang, Y.W. Tseng, J.Y. Chen, Y.C. Kuo, Dielectric properties of high-Q $(Mg_{1-x}Zn_x)_{1.8}Ti_{1.1}O_4$ ceramics at microwave frequency, J. Eur. Ceram. Soc. 163 (2012) 2365–2371.
[2] E.A. Nenasheva, S.S. Redozubov, N.F. Kartenko, I.M. Gaidamaka, Microwave dielectric properties and structure of ZnO-Nb_2O_5-TiO_2 ceramics, J. Eur. Ceram. Soc. 31 (2011) 1097–1102.
[3] R. Lowndes, F. Azough, R. Cernik, R. Freer, Structures and microwave dielectric properties of $Ca_{(1-x)}Nd_{2x/3}TiO_3$ ceramics, J. Eur. Ceram. Soc. 32 (2012) 3791–3799.
[4] A. Baumgarte, R. Blachnik, New $M^{2+}M^{4+}Nb_2O_8$ phases, J. Alloys. Compd. 215 (1994) 117–120.
[5] S.D. Ramarao, V.R.K. Murthy, Crystal structure refinement and microwave dielectric properties of new low dielectric loss $AZrNb_2O_8$ (A: Mn, Zn, Mg and Co) ceramics, Scr. Mater. 69 (2013) 274–277.
[6] Q.W. Liao, L.X. Li, X. Ren, X.X. Yu, Q.L. Meng, W.S. Xia, A new microwave dielectric material $Ni_{0.5}Ti_{0.5}NbO_4$, Mater. Lett. 89 (2012) 351–353.
[7] C.F. Tseng, Microwave dielectric properties of low loss microwave dielectric ceramics: $A_{0.5}Ti_{0.5}NbO_4$ (A = Z, Co), J. Eur. Ceram. Soc. 34 (2014) 3641–3648.
[8] C.F. Tseng, Microwave dielectric properties of a new $Cu_{0.5}Ti_{0.5}NbO_4$ ceramics, J. Eur. Ceram. Soc. 35 (2015) 383–387.
[9] P.P. Ma, X.Q. Liu, F.Q. Zhang, J.J. Xing, X.M. Chen, $Sr(Ga_{0.5}Nb_{0.5})_{1-x}Ti_xO_3$ low-loss microwave dielectric ceramics with medium dielectric constant, J. Am. Ceram. Soc. 98 (2015) 2534–2540.
[10] Z.L. Huan, Q.C. Sun, W.B. Ma, L.J. Wang, F. Xiao, T.K. Chen, Crystal structure and microwave dielectric properties of $(Zn_{1-x}Co_x)TiNb_2O_8$ ceramics, J. Alloys. Compd. 551 (2013) 630–635.
[11] R.D. Shannon, Revised effective ionic radii and systematic studies of interatomic distances in halides and chaleogenides, Acta. Cryst. A 32 (1976) 751–767.
[12] Q.W. Liao, L.X. Li, X. Ding, Phase constitution, structure analysis and microwave dielectric properties of $Zn_{0.5}Ti_{1-x}Zr_xNbO_4$ ceramics, Solid State Sci. 14 (2012) 1385–1391.
[13] C.H. Hsu, C.J. Huang, Preparation, structural and microwave dielectric properties of $CaLa_4(Zr_xTi_{1-x})_4O_{15}$ ceramics, J. Alloys Compd. 587 (2014) 45–49.
[14] B.H. Toby, EXPGUI, a graphical user interface for GSAS, J. Appl. Cryst. 34 (2001) 210–213.
[15] B.W. Hakki, P.D. Coleman, A dielectric resonator method of measuring inductive capacities in them millimeter range, IEEE Trans. Microw. Theory 8 (1960) 402–410.
[16] W.E. Courtney, Analysis and evaluation of a method of measuring the complex permtivity of microwave insulators, IEEE Trans. Microw. Theory 18 (1970) 476–485.
[17] Y. Kobayashiy, M. Katoh, Microwave measurement of dielectric properties of low-loss materials by the dielectric rod resonator method, IEEE Trans. Microw. Theory 33 (1985) 586–592.
[18] Y. Iqbal, A. Manan, Phase, microstructure and microwave dielectric properties of Zr-doped $SrLa_4Ti_{5-x}Zr_xO_{17}$, J. Mater. Sci: Mater. Electron. 23 (2012) 536–541.
[19] I. Abrahams, P.G. Bruce, W.I.F. David, A.R. West, Structure determination of substituted rutiles by time-of-flight neutron diffraction, Chem. Mater. 1 (1989) 237–240.
[20] M. Daturi, G. Busca, M.M. Borel, A. Leclaire, P. Piaggio, Vibrational and XRD study of the system $CdWO_4$-$CdMoO_4$, J. Phys. Chem. B 101 (1997) 4358–4369.
[21] E.S. Kim, B.S. Chun, K.H. Yoon, Dielectric properties of $[Ca_{1-x}(Li_{1/2}Nd_{1/2})_x]_{1-y}Zn_yTiO_3$ ceramics at microwave frequencies, Mater. Sci. Eng. B 99 (2003) 93–97.
[22] N.E. Brese, M. O'keeffe, Bond-valence parameters for solids, Acta. Cryst. B47 (1991) 192–197.
[23] F. Lichtenberg, A. Herrnberger, K. Wiedenmann, Synthesis structural, magnetic and transport properties of layered perovskite-related titanates, niobates and tantalates of the type $A_nB_nO_{3n+2}$. $A'A_{k-1}B_kO_{3k+1}$ and $A_mB_{m-1}O_{3m}$, Prog. Solid. State. Chem. 36 (2008) 253–287.
[24] H.T. Wu, Z.B. Feng, Q.J. Mei, J.D. Guo, J.X. Bi, Correlations of crystal structure, bond energy and microwave dielectric properties of $AZrNb_2O_8$ (A = Z, Co, Mg, Mn) ceramics, J. Alloys Compd. 648 (2015) 368–373.
[25] A. Glamazda, K.Y. Choi, P. Lemmens, W.S. Choi, H. Jeen, T.L. Meyer, H.N. Lee, Structural instability of the CoO_4 tetrahedral chain in $SrCoO_{3-\delta}$ thin films, J. Appl. Phys. 118 (2015) 085313–085317.
[26] S. Solomon, D.B. Dhwajam, G.R. Remya, A. John, J.K. Thomas, Fabrication and characterization of xPrTiTaO$_6$-(1-x)YTiNbO$_6$ microwave ceramic composites, J. Alloys. Compd. 504 (2010) 151–154.
[27] P.S. Narayanan, Raman spectrum of rutile (TiO_2), Proc. Indian Acad. Sci. 32 (1950) 279–283.
[28] G. Murtaza, S.S. Hussain, N.U. Rehman, S. Naseer, M. Shafiq, M. Zakaullah, Carburizing of zirconium using a low energy Mather type plasma focus, Surf. Coat. Technol. 205 (2011) 3012–3019.
[29] S. Solomon, A. George, J.K. Thomas, A. John, Preparation characterization, and ionic transport properties of nanoscale $Ln_2Zr_2O_7$ (Ln = Ce, Pr, Nd, Sm, Gd, Dy, Er, and Yb) energy materials, J. Electron. Mater. 44 (2015) 28–37.
[30] S.D. Ramarao, S.R. Kiran, V.R.K. Murthy, Structural lattice vibrational, optical and microwave dielectric studies on $Ca_{1-x}Sr_xMoO_4$ ceramics with scheelite structure, Mater. Res. Bull. 56 (2014) 71–79.
[31] N. Imanaka, M. Itaya, T. Ueda, G. Adachi, Tetravalent Zr^{4+} or Hf^{4+} ion conduction in NASICON type solids, Solid State Ionics 154–155 (2002) 319–323.
[32] S.D. Ramarao, V.R.K. Murthy, Structural, Raman spectroscopic and microwave dielectric studies on $Ni_{1-x}(Zn_{1/2}Zr_{1/2})_xW_{1-x}Nb_xO_4$ ceramic compounds with wolframite structure, Dalton Trans. 44 (2015) 2311–2324.
[33] R.D. Shannon, Dielectric polarizabilities of ions in oxides and fluorides, J. Appl. Phys. 73 (1993) 348–366.
[34] L.X. Li, H.C. Cai, X.X. Yu, Q.W. Liao, Z.D. Gao, Structure analysis and microwave dielectric properties of $Ca_xZn_{1-x}Sn_{0.08}Ti_{1.92}Nb_2O_{10}$ ceramics, J. Alloys Compd. 584 (2014) 315–321.
[35] J. Kato, H. Kagata, K. Nishimoto, Dielectric properties of (PbCa)(MeNb)O_3 at microwave frequencies, Jpn. J. Appl. Phys. 31 (1992) 3144–3147.
[36] W.S. Kim, T.H. Kim, E.S. Kim, K.H. Yoon, Microwave dielectric properties and far reflectivity spectra of the $(Zr_{0.8}Sn_{0.2})TiO_4$ ceramics with additives, Jpn. J. Appl. Phys. 37 (1998) 5367–5371.
[37] E.S. Kim, B.S. Chun, R. Freer, R.J. Cernik, Effects of packing fraction and bond valence on microwave dielectric properties of $A^{2+}B^{6+}O_4$ (A^{2+}: Ca, Pb, Ba; B^{6+}: Mo, W) ceramics, J. Eur. Ceram. Soc. 30 (2010) 1731–1736.

Please cite this article in press as: Y. Zhang, et al., Crystal structure and microwave dielectric characteristics of Zr-substituted $CoTiNb_2O_8$ ceramics, *J Eur Ceram Soc* (2016), http://dx.doi.org/10.1016/j.jeurceramsoc.2016.02.026